Water Air Soil Pollut (2018) 229:309
https://doi.org/10.1007/s11270-018-3962-3

Use of Rh (III)-Heteropolymolybdate as Potential Catalysts for the Removal of Nitrates in Human Drinking Water: Synthesis, Characterisation and Catalytic Performance

María A. Jaworski · Guillermo R. Bertolini · Carmen I. Cabello · Guillermo J. Siri · Mónica L. Casella

Received: 2 October 2017 / Accepted: 17 August 2018

Abstract The investigation and development of technologies to remediate water contaminated with NO_3^- are constantly increasing. An economically and potentially effective alternative is based on the catalytic hydrogenation of NO_3^- to N_2. With this objective, bimetallic $RhMo_6$ catalysts based on Anderson-type heteropolyanion $(RhMo_6O_{24}H_6)^{3-}$ were prepared and characteri3ed in order to obtain well-defined bimetallic catalyst. The catalysts were supported on Al_2O_3 with different textural properties and on silica. The heteropolyanion-support interaction was analysed by temperature-programmed reduction (TPR) and X-ray photoelectron spectroscopy (XPS). The differences obtained in activity and selectivity to the different products can be assigned to the different interaction between the $RhMo_6$ Anderson phase and the supports. The $RhMo_6$/G, (G: γ-Al_2O_3) system showed the best catalytic performance. This catalyst exhibited the lowest reduction temperature of Rh and Mo in the TPR assay and a Rh/Mo surface ratio similar to that of the original phase, as observed by XPS analysis. These studies allowed us to verify a synergic effect between Rh and Mo, through which Mo reducibility was promoted by the presence of the noble metal. The catalytic activity was favoured by the active sites generated from the Anderson phase. This fact was confirmed by comparing the activity of $RhMo_6$/G with that corresponding to a conventional catalyst prepared through successive impregnation of both Rh (III) and Mo (VI) salts.

Keywords Nitrate · Water pollution · Well-defined catalysts · Anderson phase · Hydrogenation · Synergic effect

M. A. Jaworski (✉) · G. R. Bertolini · C. I. Cabello · G. J. Siri · M. L. Casella
Centro de Investigación y Desarrollo en Ciencias Aplicadas "Dr. Jorge J. Ronco" (CINDECA), CCT-CONICET La Plata, Universidad Nacional de La Plata and Comisión de Investigaciones Científicas de la Provincia de Buenos Aires (CICPBA), calle 47 N° 257, 1900 La Plata, Argentina
e-mail: majaworski@quimica.unlp.edu.ar

M. A. Jaworski · G. J. Siri
PIDCAT-Facultad de Ingeniería (UNLP), 47 N° 257, La Plata, Argentina

C. I. Cabello
Miembro CIC, Comisión de Investigaciones Científicas y Técnicas, Provincia de Buenos Aires and Facultad de Ingeniería UNLP, La Plata, Argentina

1 Introduction

Traditionally, soils have been fertilised with NO_3^- to improve agricultural yields. Since the artificial synthesis of ammonia was achieved by the Haber process, it has been possible to produce nitrogen fertilisers, which are currently used in large quantities in agriculture (Haber and Le Rossignol 1910). As a result of this intensive use of fertilisers, NO_3^- concentration has been constantly increasing in groundwater since 1950 (Costa et al. 2012).

The intake of water containing NO_3^- has adverse effects on human health, so maximum tolerable levels have been established for NO_3^- in water for human consumption (45 ppm according to the US Environmental Protection Agency). NO_3^- is harmful because it is reduced

Published online: 01 September 2018

to NO_2^- in the human body and NO_2^- favours the development of methemoglobinaemia, which is a deficiency of oxygen in blood that can put life in danger, especially for children under 6 months ("blue baby syndrome"). When NO_3^- is transformed to NO_2^- in the human body, other reactions can take place. NO_2^- could react with amine compounds to form the so-called N-nitrosamines (NOC, N-nitroso compound), some of which have proven to be mutagenic and carcinogenic (Citak and Sonmez 2010).

Nitrate is a stable and highly soluble ion with low tendency to co-precipitation and adsorption. These properties make it difficult to be removed from water. The application of technologies to remediate polluted groundwater with NO_3^- is increasing, particularly in places where alternative water supplies are unavailable. These technologies include ion exchange, reverse osmosis, electro dialysis, photocatalytic reduction, biological methods and catalytic reduction (Ding et al. 2017; Kim et al. 2016).

The best technique to remove NO_3^- from contaminated groundwater is the one that can convert this anion into N_2. Since Vorlop and Tacke (1989) developed the NO_3^- reduction to N_2 using bimetallic catalysts in the presence of a reducing agent, numerous studies have been carried out in order to find the most efficient catalysts for that process. One of the most accepted mechanisms for this reaction establishes that NO_3^- can only be hydrogenated using bimetallic catalysts if an inert support is used, while NO_2^- and other reaction intermediates are reduced by monometallic catalysts (Barrabés and Sá 2011). For this reason, the most studied catalytic systems are bimetallic catalysts, composed of a noble metal (Pd, Pt, Rh) that can easily chemisorb H_2 and a second metal, such as Cu, Ni, Fe, Sn or In (Barrabés and Sá 2011; Bae et al. 2013; Choi et al. 2013). In these catalysts, the bimetallic sites allow the reduction of NO_3^- to NO_2^-, which is then reduced to N_2 or over-reduced to NH_4^+ on monometallic sites, as shown in the following equations:

$$NO_3^- + H_2 \rightarrow NO_2^- + H_2O \quad (1)$$

$$2NO_2^- + 3H_2 \rightarrow N_2 + 2H_2O + 2OH^- \quad (2)$$

$$NO_2^- + 3H_2 \rightarrow NH_4^+ + 2OH^- \quad (3)$$

Different studies reveal that the activity and selectivity to N_2 in NO_3^- removal reaction depends on the interaction between the metals forming the active phase (a fact that can be controlled by the preparation method), the nature of the promoter, the metal/promoter ratio and the operating conditions (Soares et al. 2010).

In this sense, numerous recent studies have focused mainly on the development of new catalysts with a defined chemical composition and an orderly distribution of the elements of the active phase that are active in the reduction of nitrate. The methodologies tested included the preparation and use of $PtSn/\gamma\text{-}Al_2O_3$ bimetallic catalysts prepared by Surface Organometallic Chemistry on Metals techniques (Jaworski et al. 2013), preparation of Pd and In catalysts by sequential electroless plating on activated carbon felts (Zoppas et al. 2016) and more recently, $PdAg/SiO_2\text{-}NH_2$ catalyst were developed by a controlled surface reaction to load Ag and create PdAg alloy nanoparticles on NH_2 surface-modified SiO_2 catalyst support ($SiO_2\text{-}NH_2$) (Ding et al. 2017).

The heteropolyoxomolybdates forming Anderson phases of Co, Ni or Rh have emerged as interesting precursors in heterogeneous catalysts in various processes and have begun to replace different conventional oxidic precursors improving the efficiency and the environmental conditions of various catalytic processes (Mizuno and Misono 1998; Pettiti et al. 2001). The planar structure of the heteropolyanion and its redox and acidity properties are relevant factors in the heteropolyanion-support interaction process, which produces an active surface with an ordered distribution and uniform deposit of metallic elements, thus favouring the synergistic effect between the transition metal and Mo. In Fig. 1, the polyhedral structure of Rh (III)-heteropolyoxomolybdate of formula

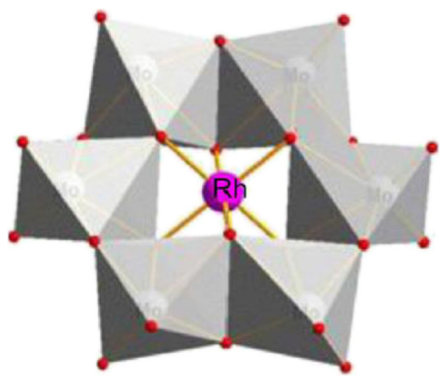

Fig. 1 Representation of the structure corresponding to the planar-type Anderson phase Rh (III) hexamolybdate $[RhMo_6O_{24}H_6]^{3-}$

$[RhMo_6O_{24}H_6]^{3-}$ is shown. Its configuration (D_{3d} planar symmetry) consists of a central Rh (III) heteroatom surrounded by six octahedral MoO_6 groups. Each MoO_6 shares an edge with each of its two neighbouring MoO_6 and another edge with the Rh $(OH)_6$ octahedron (Cabello et al. 2000).

Recently, bimetallic RhMo precursors generated from heteropolyoxomolybdates of the Anderson-type structure with formula $(NH_4)_3[RhMo_6O_{24}H_6].7H_2O$ supported on γ-Al_2O_3 or modified clays have been successfully employed in the hydrogenation of cinnamaldehyde to hydrocinnamaldehyde (Bertolini et al. 2013, 2016).

Regarding the limited publications about the application of heteropolycompounds in catalytic hydrogenation in aqueous solutions, this work aims to study the catalytic hydrogenation of NO_3^- in water with bimetallic RhMo catalysts prepared using a Rh (III) and Mo (VI) Anderson phase. The performance of the catalysts is a combination of the nature and structure of the active phase and the chemical and textural characteristics of the support so the discussion is also focused on the nature of the supports employed.

2 Experimental

2.1 Preparation of the Supports

An alumina support (B) was prepared in our laboratory starting from the precursor "gibbsite" (Al $(OH)_3$). Different calcination temperatures (in the range 480–900 °C) were tested in order to obtain a support with suitable textural properties.

To analyse the effect of the support, three other supports were selected: two commercial aluminium oxides of different origin and another one based on silica. The alumina supports were a commercial γ-Al_2O_3 (Esferalite) and one α-Al_2O_3, named G and A, respectively.

In order to condition the silica-based support, the commercial silica (Degussa Aerosil 200) was submitted to a procedure published by Dalmon and Martin (1980). Approximately, 20 g of the material was treated with 100 mL of aqueous $NH_4(OH)$, reaching a pH of 10.6, to improve its hydrophilic and textural properties. The system was kept at 25 °C in a thermostatic bath for 30 min. The solid was then separated from the solution by filtration and dried in an oven for 24 h at 105 °C. After this treatment, the surface of the support is composed of "silanol" groups SiO_2-OH, increasing its specific surface area, pore volume and pore diameter. This support was designated as S.

2.2 Anderson Phase Preparation

The procedure to obtain the Anderson phase $(NH_4)_3[RhMo_6O_{24}H_6].7H_2O$ (hereafter, $RhMo_6$) was as follows: 20 mL of a solution containing 0.70 g of $(NH_4)_6[Mo_7O_{24}].4H_2O$ (hereafter, HMA), previously heated to $T < 80$ °C to facilitate its dissolution, and 10 mL of an aqueous solution containing the stoichiometric amount of $RhCl_3.H_2O$ were mixed. The pH was adjusted to 5–6 with an NH_4Cl solution. The system was kept at room temperature for several days until the appearance of the corresponding precipitate. Then, the solid was filtered, washed and dried in an oven at 80 °C.

2.3 Catalyst Preparation

Starting from the Anderson phase, the following catalysts were prepared: $RhMo_6$/B, $RhMo_6$/G, $RhMo_6$/A and $RhMo_6$/S using the equilibrium-adsorption method. A $RhMo_6$ aqueous solution having a Mo concentration of 10 mg/mL was employed in order to obtain catalysts with 6 wt% Mo and 1 wt% Rh adsorbed on the supports. After the impregnation process, the catalyst was separated from the solution by centrifugation and then dried in an oven at 80 °C.

In addition, some reference catalysts were prepared. (i) A conventional bimetallic catalyst (designated as RhMo/G) prepared by successive impregnation, using HMA and $RhCl_3.6H_2O$. Appropriate amounts of each salt were dissolved in water in order to obtain a catalyst with Rh and Mo contents similar to those present in the $RhMo_6$/G catalyst. (ii) Monometallic Rh/G and Mo/G catalysts prepared by a conventional impregnation procedure, using $RhCl_3$ and HMA aqueous solutions, respectively.

Before being used, all the catalysts were pretreated in H_2 flow at 350 °C.

2.4 Characterisation of the Anderson Phase and of the Prepared Catalysts

The textural properties of the supports were determined from the N_2 adsorption–desorption isotherms at − 196 °C in Micromeritics ASAP 2020 equipment.

The specific surface area (S_{BET}) was determined by the Brunauer, Emmett and Teller (BET) method (Brunauer et al. 1985). The samples were pretreated under vacuum in two stages of 1 h at 100 and 300 °C. The pore distribution was determined by the Barrett–Joyner–Halenda (BJH) method (Barrett et al. 1951) from the analysis of the micropore isotherm by the *t* test (Lippens and de Boer 1965) taking the curve of Harkins and Jura (1994); the total pore volume was determined by the rule of Gurvitsch (1914).

The Mo and Rh contents were determined by atomic absorption spectrometry (AAS-equipment Varian AA 240) on the initial (C_i) and final (C_f) solutions. The adsorbed concentrations of Mo and (C_a^{Mo} or C_a^{Rh}) were calculated from experimental C_i and C_f data, taking into account the volume of the impregnated solution and the mass of the support (m) according to the expression:

$$C_a = \left\{ \frac{(C_i - C_f)V}{m} \right\} 100$$

The temperature-programmed reduction (TPR) patterns were obtained in a flow system with a mixture of 10 vol.% H_2 and 90 vol.% N_2 volume (20 cm^3/min), by heating from room temperature up 850 °C at 10°/min in a Quantasorb Jr. (Quantachrome) equipment.

Scanning electron microscopy (SEM) with EDS analysis was performed in a Microscope Philips SEM 505 with a dispersive energy system for microanalysis (EDAX 9100).

The XRD patterns were collected in a Philips PW-1390 equipment using a Cu Kα radiation source (λ = 1.5406 Å) with 40 kV and 20 mA. Nickel filter and scanning angles in the 2θ range between 5 and 60° at a scanning rate of 2°/min were used. Crystalline phases were identified using the Joint Committee on Powder Diffraction Standards (JCPDS) files (Joint Comité for Powder Diffraction Standards).

X-ray photoelectron spectroscopy (XPS) spectra were recorded on a SPECS multi-technique analysis instrument spectrometer equipped with a dual X-ray Mg/Al source and a PHOIBOS 150 hemispherical analyser in the fixed analyser transmission (FAT) mode. The spectra were obtained with a pass energy of 30 eV and an Mg anode operated at 200 W. The pressure during the measurement was lower than 2×10^{-8} mbar. The sample was placed on the sample holder of the instrument, reduced to 350 °C for 10 min in a 5% H_2 in Ar flow and evacuated to ultra-high vacuum for at least 2 h before the measurement. The Rh_{3d}, Mo_{3d}, O_{1s} and Al_{2p} regions were processed by a computer. Electron binding energies (BE) were referenced to the C_{1s} peak at 284.6 eV. The intensity ratio I_{Me}/I_{Al} (for Me = Rh or Mo) was obtained from peak area determination by integration of the appropriate peaks. To assess a quantitative relationship between the XPS peak intensity ratio and surface composition, the experimental results were corrected with the values predicted by Scofield's sensitivity factors (Wagner et al. 1981).

The FT-IR spectra of pure Anderson phase and of the prepared catalysts were obtained in the 400–4000 cm^{-1} wavenumber range using KBr pellets in a Thermo Bruker IFS 66 FT-IR spectrometer.

Raman spectra were collected on powder samples at room temperature in the back-scattering geometry with an in Via Renishaw spectrometer equipped with an air-cooled CCD detector and a super-Notch filter. The emission line at 514.5 nm from an Ar^+ ion laser was focused on the sample under a Leica DLML microscope using a × 20 objective. Five 20-s accumulations were attained for each sample with an incident beam power of about 5 mW. The spectral resolution was 2 cm^{-1}, and the spectra were calibrated using the 520.5 cm^{-1} line of a silicon wafer.

2.5 Catalytic Test

The hydrogenation of NO_3^- was carried out in a semi-batch Pyrex reactor. In a typical run, the catalysts were previously reduced under a H_2 flow at 350 °C for 2 h and loaded in the reactor that contained a 100 ppm NO_3^- solution in degassed distilled water. The experiment was carried out for 6 h at atmospheric pressure, 25 °C, with a 400 mL min^{-1} H_2 flow. To monitor the reaction progress, 1 mL samples were taken periodically. The samples were filtered and then analysed in an ion chromatograph (Metrohm 790 Personal IC) to determine NO_3^- and NO_2^- concentrations. A solution of $NaHCO_3$ 1.0 mM and Na_2CO_3 3.2 mM was used as the mobile phase, and the flow rate was set at 7 mL/min. Ammonium ions were determined by UV-Vis spectrophotometry (UV-Vis Thermo Spectronic Helios Gamma), following a modified

Berthelot method (Marchesini et al. 2010). The selectivity to NO_2^- ($S_{NO_2^-}$ %), NH_4^+ ($S_{NH_4^+}$ %) and N_2 (S_{N_2} %) after 300 min (t) of reaction was calculated with the following equations:

$$S_{NO_2^-}(\%) = \frac{\left[NO_2^-\right]_t}{\left[NO_3^-\right]_{inicial} - \left[NO_3^-\right]_t}{}^{*} 100\% \quad S_{NH_4^+}(\%) = \frac{\left[NH_4^+\right]_t}{\left[NO_3^-\right]_{inicial} - \left[NO_3^-\right]_t}{}^{*} 100\%$$

$$S_{N_2}(\%) = 100 - S_{NO_2^-}(\%) - S_{NH_4^+}(\%)$$

3 Results and Discussion

The term *alumina* is generally used to identify some of the crystalline forms of aluminium oxide (Al_2O_3), aluminium hydroxide (Al $(OH)_3$) or aluminium hydroxide oxide (AlO (OH)) (Gitzen 1970). Aluminas occur in nature as hydroxides or hydrated mineral oxides (bauxite), which through hydrotreating processes are transformed into gibbsite or bayerite, which happen to be the precursors of the so-called transition aluminas. Among them, the most important is *gibbsite*, which is usually obtained through the Bayer process (Zhao and Chen 2003). In this process, bauxite ore is heated in a pressure vessel along with a sodium hydroxide solution at a temperature of 150 to 200 °C, in order to obtain a sodium aluminate solution. After the separation of the insoluble impurities, the remaining solution is diluted with water in order to cause the hydrolysis and precipitation of *gibbsite*. *Gibbsite* is transformed into different types of aluminium hydrous oxides depending on the temperature and time of the process, and also on the treating atmosphere, giving rise to different crystalline phases along with the elimination of water. These so-obtained phases are called "transition aluminas", each one of them exhibiting characteristic properties: crystal structure, specific surface, grain size, etc. (Zhao and Chen 2003). In the present work, the sample thermally treated at 550 °C was selected to continue the rest of the experiments due to the fact that this support (designated as B) was the one with which the best textural characteristics (high S_{BET} and suitable pore size) were found.

The textural properties of the supports used in this paper are displayed in Table 1. Supports designated as G and A have textural properties corresponding to the traditional values found in the literature for these kinds of aluminas (Vieira Coelho et al. 2008). After the treatment at high pH with aqueous ammonia, the silica support (S) resulted in a solid with a high S_{BET} and high porosity compared with the untreated Aerosil Degussa (65m^2/g and 0.14 cm^3/g, respectively).

In Fig. 2, the N_2 adsorption isotherms for S, G and B supports are shown. These isotherms have been analysed in the light of the newest IUPAC Technical Report (Thommes et al. 2015). Taking into account these recommendations, physisorption isotherms of G and B supports correspond to Type IVa isotherms, typical of mesoporous adsorbents. The adsorption behaviour in mesopores is determined by the adsorbent–adsorbate interactions and also by the interactions between the molecules in the condensed state. In Type IVa isotherm, capillary condensation is accompanied by hysteresis. The observed hysteresis loops for G and B supports are of Type H2 and can be attributed either to pore-blocking/percolation in a narrow range of pore necks or to cavitation-induced evaporation (Thommes and Cychosz 2014).

Table 1 Nomenclature and textural properties of the supports

Support	Nomenclature	S_{BET} (m^2/g)	Pore volume (cm^3/g)
γ-Al_2O_3	G	255	0.65
Al $(OH)_3$ calcined at 550 °C	B	159	0.24
α-Al_2O_3	A	10	0.05
SiO_2	S	180	0.76

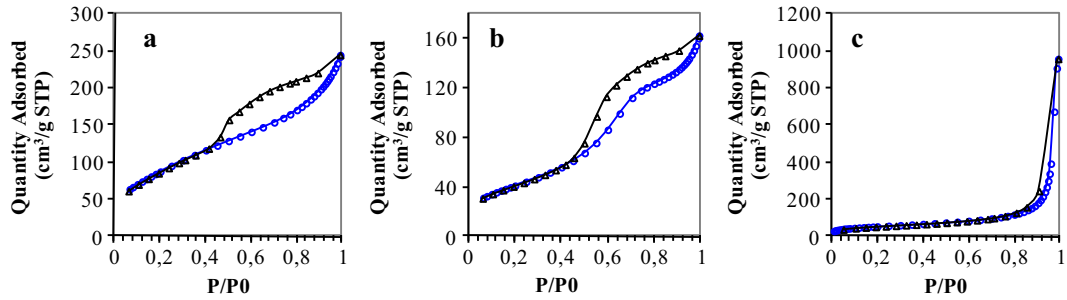

Fig. 2 N_2 adsorption/desorption isotherms of G (**a**), B (**b**) and S (**c**) supports

On the other hand, the S support presents a Type V isotherm, typical of solids with a relatively weak adsorbent–adsorbate interaction. The observed hysteresis corresponding to a Type H1 loop is found in materials that exhibit a narrow range of uniform mesopores, as for instance in template silicas, some controlled pore glasses and ordered, mesoporous carbons. The steep, narrow loop characteristic of this type of hysteresis is assigned to a delayed condensation on the adsorption branch. However, Type H1 hysteresis has also been found in networks of ink-bottle pores where the width of the neck size distribution is similar to the width of the pore/cavity size distribution (Thommes and Cychosz 2014).

The X-ray diffraction patterns of G and B supports are depicted in Fig. 3(a, b). The diffraction signals for these supports at $2\theta = 15°$, 29.4°, 39.0° and 48.0° (PDFWIN: 89-7717) account for the different degree of crystallinity of the solids. Figure 3(c) presents the XRD pattern of S support, which corresponds to an amorphous silica, as reported in the international database (PDFWIN: 38-0448).

The $RhMo_6$ Anderson phase employed in this paper has been extensively characterised in previous work of our research group by different techniques including SEM-EDS, XRD, FT-IR and Raman microprobe. The main results of its characterisation can be summarised as follows: SEM-EDS microscopy showed that the synthesised crystals of $(NH_4)_3[RhMo_6O_{24}H_6]\cdot 7H_2O$ (pale orange) were similar to other Anderson phases such as $CoMo_6$, $CrMo_6$ and $AlMo_6$. The XRD pattern of powder samples showed that the Rh phase was isomorphous to phases containing a trivalent metal as heteroatom. From the EDS semi-quantitative analysis, a good agreement was observed between the Rh and Mo contents obtained experimentally (15.91 wt% and 84.09 wt% of Rh (III) and Mo (VI), respectively) and the theoretical values 15.16 wt% for Rh (III) and 84.83 wt% for Mo (VI) (Bertolini et al. 2013; Cabello et al. 2006).

In order to test the potentiality of $RhMo_6$ phase in the catalytic denitrification of water, it was supported on the different selected solids, giving rise to $RhMo_6$/B, $RhMo_6$/G, $RhMo_6$/A and $RhMo_6$/S catalysts. The quantitative analysis of Rh and Mo was conducted by AAS, and the results are summarised in Table 2, together with the semi-quantitative EDS values.

Both alumina-supported catalysts ($RhMo_6$/B and $RhMo_6$/G) prepared by the equilibrium-adsorption method contained ca. 6 wt% Mo and 1.5 wt% Rh, in agreement with the previously prepared $RhMo_6$-based supported catalysts (Bertolini et al. 2013). The concentration of Rh and Mo adsorbed on the support not only depends on the initial concentration of the starting solutions, but also on the interaction of the Anderson phase with the support. Thus, the similar octahedral coordination geometry of Rh (III) in the Anderson phase and of the Al (III) cations of the alumina support suggests an effective interaction of the $RhMo_6$ phase with the alumina support, and a high affinity or possibility of

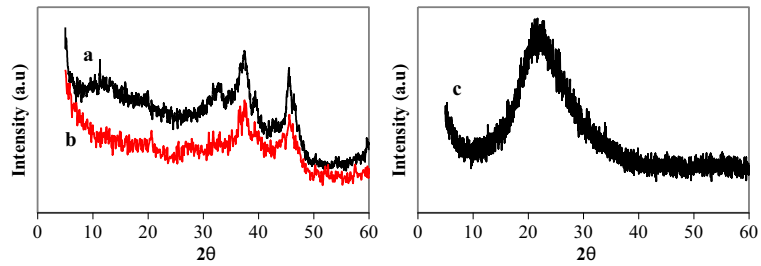

Fig. 3 XRD patterns of G (**a**); B (**b**) and S (**c**) supports

Table 2 Values for Rh and Mo concentration obtained by AAS and EDS semi-quantitative analysis

Catalyst	Values obtained by AAS (%)		Values obtained by EDAX (%)	
	Rh	Mo	Rh	Mo
$RhMo_6/G$	1.50	6.00	9.45	50.62
$RhMo_6/B$	1.40	5.70	7.14	41.5
$RhMo_6/S$	0.12	0.58	1.02	4.23

exchange of Rh (III) and Al (III). The ionic radii of both cations in the octahedral coordination are similar (0.53 Å and 0.66 Å for Al (III) and Rh (III), respectively) allowing a certain degree of substitution for one another on the support surface.

The values of Mo and Rh obtained for $RhMo_6/S$ were much lower: 0.58 wt% and 0.12 wt%, respectively. However, the values found by the semi-quantitative method were 4.23% for Mo and 1.02% for Rh for the silica support. The lower adsorption of the Anderson phase on the silica support can be explained by the PI (isoelectric point) of the supports and the preferential impregnation of the heteropolyanion. The PI value for silica is 2 and indicates the acidic nature of the support, which means that at pH > 2 its surface mostly has negative charges; however, this becomes significant at pH ≥ 5. This is the pH value of the aqueous solution of the heteropolyanion of interest, in which this species is stable. So the impregnation of a polyanion such as $[RhMo_6O_{24}\ H_6]^{-3}$ does not produce an effective exchange, as was demonstrated by the values obtained by the AAS and EDS methods. Also, Si (IV) has a ionic radius of 0.24 Å in a tetrahedral environment, which does not favour its exchange with Rh (III), as in the case of alumina.

XRD patterns of the catalysts were obtained. The profile of the $RhMo_6/G$ catalyst shows the diffraction lines characteristic of the γ-Al_2O_3 support (PDFWIN: 89-7717). Unlike support B, which presented the signals corresponding to γ-Al_2O_3, it showed a diagram with well-defined signals characteristic of *boehmite* when it was impregnated with the Anderson phase generating the $RhMo_6/B$ catalyst. According to Rinaldi et al. (2006), the hydration of a gamma alumina phase may result in the formation of aluminium oxyhydroxide and trihydroxide (*boehmite* and *bayerite*). So, it is possible to speculate that the impregnation in equilibrium of the support B with an aqueous solution of $RhMo_6$ resulted in the hydration of the alumina, stabilising the *boehmite* phase. In both catalysts, structures containing neither Rh nor Mo were observed, suggesting a good dispersion or the presence of small metallic particles not detected by XRD. The XRD analysis of the $RhMo_6/S$ catalyst did not show any peaks corresponding to Rh and/or Mo phases, in agreement with the low concentration of both metals deposited on the silica support.

Vibrational spectroscopy is a particularly useful technique for identifying the structure of the Anderson phases through the analysis of the vibrational modes of their typical bonds. Both the bulk Anderson phase and the $RhMo_6/G$ catalyst were analysed by FT-IR and Raman microprobe techniques. The FT-IR spectra of both samples are presented in Fig. 4(a, b). The main features typical of Anderson structure appear at 943 (ν_s), 915 cm^{-1} and 887 cm^{-1} (ν_{as}) (Mo–Ot vibrations), 642 cm^{-1} (Mo–O bridge bonds) and 566 cm^{-1} (Rh–O stretching) (Cabello et al. 2002). For the $RhMo_6/G$ catalyst, the bands are less intense than those of the pure phase, but are still possible to observe them.

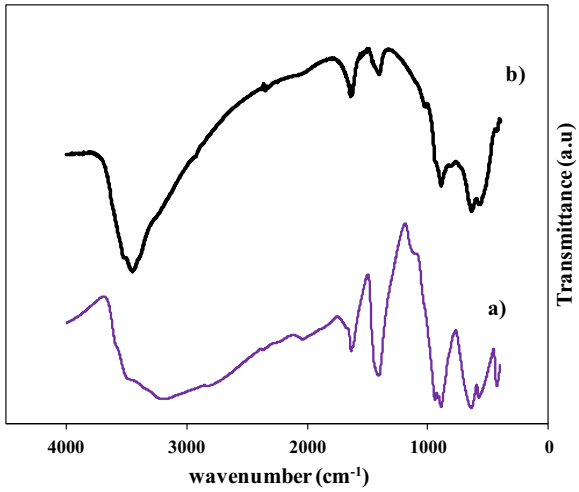

Fig. 4 FTIR spectra of $RhMo_6$ (**a**) phase and $RhMo_6$ /G catalyst (**b**)

Table 3 Binding energies (eV) and surface composition of the pure and supported $RhMo_6$ phase

Catalyst	$Rh3d_{5/2}$/eV	$Mo3d_{5/2}$/eV	Composition	
			$(nRh/nMo)^S$	$(nRh/nMo)^A$
$RhMo_6$	310.8	233.0	0.17	0.167
$RhMo_6/G$	309.4	232.7	0.23	0.223
$RhMo_6/B$	309.1	232.6	1.22	0.229

[S] XPS-derived values

[A] Analytical data (phase $RhMo_6$ for SEM/EDS, catalysts by AAS)

The Raman technique is especially interesting because it allows characterising alumina-supported Anderson phases more clearly than other techniques, showing the structure preservation. Using this technique, the preservation of the $RhMo_6$ phase structure could be verified for the $RhMo_6/G$ catalyst. The same signals appear in the spectra of the pure and supported phases, with the sole difference that the main line corresponding to the symmetric stretching mode of the $Mo–O_{2t}$ terminal bonds presents a remarkable band broadening and a shift to lower frequencies as a result of its interaction with the support (Bertolini et al. 2013).

XPS analysis provides information on the chemical state and the degree of dispersion of surface species in the supported catalysts. The data of pure phase $RhMo_6$ (Table 3) revealed signals of $Rh3d_{5/2}$ at 310.8 eV and $Mo3d_{5/2}$ at 233.0 eV, corresponding to Rh (III) and Mo (VI), respectively. Due to the overlap of the N_{1s} band with the component $Mo3p_{3/2}$, the status and the amount of N could not be determined. The chemical composition of the surface, nRh/nMo = 0.17, derived from the Rh/Mo intensity ratio, is in excellent agreement with the composition of the bulk, nRh/nMo = 0.167 (Bertolini et al. 2013).

The $RhMo_6/G$ and $RhMo_6/B$ systems showed a shift towards lower binding energy (BE) values. In the catalyst with the best catalytic performance, $RhMo_6/G$, a 1.4 eV shift towards lower values of the Rh $3d_{5/2}$ binding energy is observed (Fig. 5a), indicating that Rh is in a metallic state (García-Fierro et al. 1988, Nyholm R., Martensson N. J. Phys. C. 13, L279 (1980)). The Mo $3d_{5/2}$ band of the catalysts also showed a slight shift to lower BE values when compared to the pure Anderson phase, suggesting the presence of MoO_x species with lower oxidation states ($2 < x < 3$) (Fig. 5b) (Kim et al. 1974).

As to the surface composition, in the $RhMo_6/G$ catalyst, the Rh/Mo ratio was very similar to that obtained by AAS, revealing that the Rh/Mo ratio in the deposited phase did not change. The $RhMo_6/B$ catalyst showed surface enrichment in Rh, indicating that the Rh environment changed in one of the preparation steps.

TPR is an interesting method to analyse the heteropolyanion $RhMo_6$-support interaction and the influence of the heteroatom Rh on the reducibility of Mo. The diagrams for HMA, the $RhMo_6$ pure phase, the catalysts $RhMo_6/G$, $RhMo_6/B$, $RhMo_6/S$ and the catalyst prepared by successive impregnations (RhMo/G) are shown in Fig. 6.

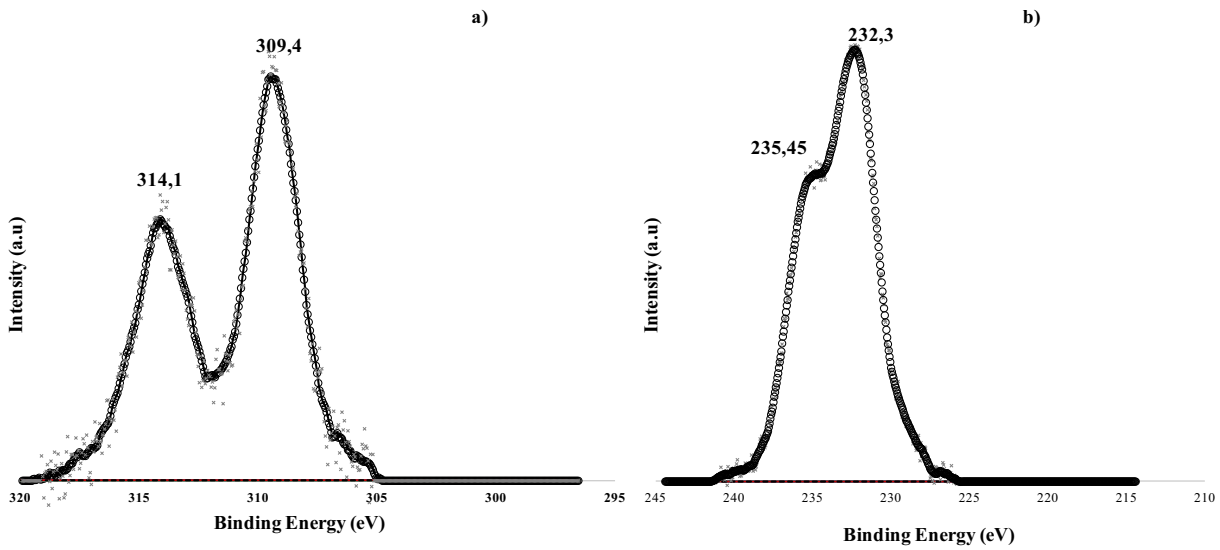

Fig. 5 XPS spectra of $RhMo_6$ phase (**a**) and $RhMo_6/G$ catalyst (**b**)

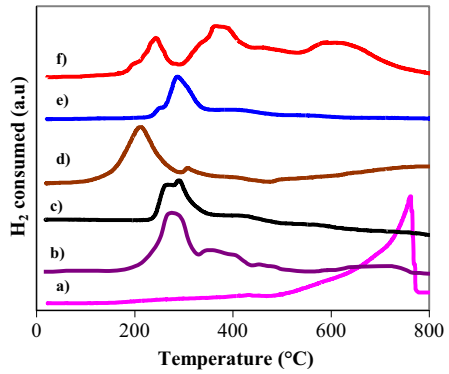

Fig. 6 TPR profile for HMA (a), $RhMo_6$ pure Anderson phase (b), $RhMo_6$/B (c), $RhMo_6$/G (d), $RhMo_6$/S (e) and RhMo/G (f) catalysts

In an H_2 reducing atmosphere, at elevated temperatures, Mo (VI) undergoes a complex process of reduction that is influenced by the metallic environment, the crystal structure of the original phase, the partially reduced phase and the presence of an additional metal in the structure (Cabello et al. 1994). The TPR profile for HMA was added for comparative purposes. There is a very low intensity peak at approximately 430 °C and another intense peak at approximately 760 °C, corresponding to two reduction stages: (Mo (VI) → Mo (IV) → Mo°) respectively. For the $RhMo_6$ phase, the TPR diagram presents a very intense signal at 285 °C, several signals of low intensity between 390 and 500 °C and another at 730 °C. The first peak at 285 °C is attributed to the reduction of Rh (III) → Rh°. If it is considered that the reduction of Rh_2O_3 occurs at 135 °C (Bouras 2003), this effect can be assigned to greater stability in the condensed metal structure. The other signals correspond to the reduction of Mo, which occurs at temperatures below those observed for the reduction of HMA. This behaviour is attributed to the synergistic effect that exists in the Anderson phase, which could also be verified through the TPR of other Anderson phases (Cabello et al. 1994).

The $RhMo_6$/G catalyst displayed H_2 consumption peaks at 210 °C and 310 °C, and showed a broad signal approximately at 730 °C, while the $RhMo_6$/B catalyst showed a broad H_2 consumption peak in the range 210 °C–350 °C, with a very similar profile to that of the $RhMo_6$ pure phase. For the $RhMo_6$/S catalyst, a strong signal around 290 °C was observed. Previous XRD and SEM-EDX characterizations of the pure phase treated at the main peak temperature revealed the simultaneous presence of Rh° and different Mo phases (Mo° and MoO_2) (Cabello et al. 2002). The strong initial hydrogen consumption for the catalysts analysed involves not only the reduction of Rh (III) to Rh^0 but also the partial reduction of Mo, which normally occurs at temperature close to 700 °C for a species such as ammonium heptamolybdate. This behaviour implies a promoter effect of Rh on Mo reducibility, as has recently been reported (Bertolini et al. 2013). In that, it was found that the high reducibility of $RhMo_6$ can be associated with the oxidising character of the heteroatom (E°Rh (III)-Rh° = 0.44 V) that promotes the activation of H_2, which in turn affects the stability of Mo (VI), whose reduction begins at lower temperature.

The catalysts prepared using the $RhMo_6$ phase were evaluated in the reaction of NO_3^- removal from water using H_2 as a reducing agent. Figure 7 shows that all catalysts containing the $RhMo_6$ phase were active in the removal of NO_3^-. The order of decreasing activity was the following: $RhMo_6$/G > $RhMo_6$/S > $RhMo_6$/B > $RhMo_6$/A. In all the catalysts tested, the pH increase from 5.5 to 10. The selectivity to N_2 (Table 4) was higher than 90% in the three catalysts supported on alumina ($RhMo_6$/G, $RhMo_6$/B, $RhMo_6$/A). For the catalyst supported on SiO_2, the selectivity was low, around

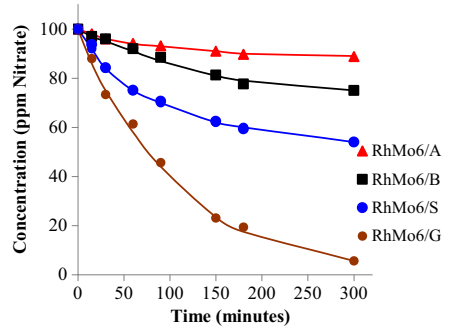

Fig. 7 Concentration of NO_3^- as a function of time for the catalysts containing the $RhMo_6$ phase

Table 4 Concentration and selectivity to the products at the end of the reaction*

Catalyst	Final ppm NO_3^-	Final ppm NO_2^-	Final ppm NH_4^+	$S_{NO_2^-}$ %	$S_{NH_4^+}$ %	S_{N_2} %
$RhMo_6$/A	89	0.8	0.04	7.3	0.36	92.3
$RhMo_6$/S	54	16.5	0.20	36	0.43	63.6
$RhMo_6$/B	75	2	0.16	8	0.64	91.4
$RhMo_6$/G	6	1.2	0.09	1.3	0.10	98.6

*The determinations were made at 300 min

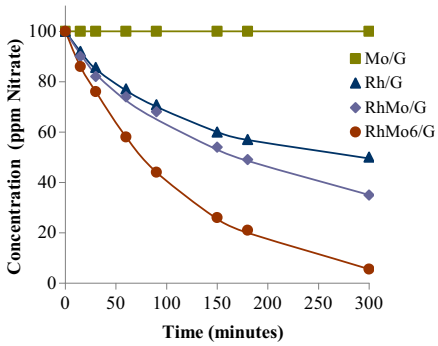

Fig. 8 Concentration of NO_3^- as a function of time for the monometallic and bimetallic catalysts containing Rh and Mo

64%, compared to that of the alumina-based materials. For all the catalysts, the concentration of NH_4^+ was below the limit values set by the European Community (0.5 ppm). In addition, a rapid and substantial pH increase from the beginning of the reaction was observed for all the analysed catalysts.

As aforementioned, the characterisation of the supports and catalysts showed differences in the textural characteristics with the consequent different adsorption of the Anderson phase. Thus, for the $RhMo_6$/A catalyst, the activity was low because of its low S_{BET} and pore volume that inhibit the effective adsorption of the heteropolyanion.

The study using transition aluminas of different textural properties (supports G and B) showed that these properties had a significant influence on the adsorption of the active phase and then on the catalytic performance. The $RhMo_6$/G catalyst showed high catalytic activity, with only 6 ppm of NO_3^- remaining at the end of the reaction (300 min), while for the system $RhMo_6$/B, at the same time, 75 ppm of NO_3^- remained unconverted.

In the $RhMo_6$/B catalyst, XPS results revealed a change in the Rh-Mo surface ratio and Rh surface enrichment. Thus, on partially losing their Mo environment, Rh atoms would act as a monometallic catalyst, i.e., with lower activity and higher selectivity to NO_2^- and NH_4^+ than the $RhMo_6$/G catalyst.

Finally, the $RhMo_6$/S catalyst showed low capacity to eliminate NO_3^- and low selectivity to N_2, compared to the $RhMo_6$/G catalyst. Considering that the IP values of G and S supports are different, the NO_3^- removal rate was expected to be different as well. Working at a controlled pH of 5.5, Marchesini et al. (2008) found that the NO_3^- removal rate was higher for the Al_2O_3 support. This research group attributed the lower activity of the SiO_2 support in NO_3^- removal to its lower IP value (3.2) compared to that of Al_2O_3 (7.7), which would decrease the adsorption efficiency of NO_3^- ions on the support.

The results obtained for the activity and selectivity towards N_2 (Fig. 7 and Table 4) show that the catalyst with the best catalytic performance was $RhMo_6$/G. With the purpose of analysing whether the catalytic activity is favoured by the Anderson phase, a RhMo/G catalyst was prepared for comparison purposes by the method of successive impregnation, as was described in the experimental section. In addition, the monometallic Rh/G and Mo/G catalysts were evaluated in the studied reaction.

The results for the removal of NO_3^- from water using the catalysts containing Rh and Mo are shown in Fig. 8. The Mo/G catalyst is practically inactive in the removal of NO_3^-. Contrary to what was reported in the literature for monometallic catalysts prepared over an inert support such as γ-Al_2O_3, the Rh/G catalyst is active in removing NO_3^- (Jaworski et al. 2013). In addition, this catalyst has a good selectivity towards N_2 but greater selectivity towards NO_2^- (Table 5) than the other catalysts tested. Probably the high hydrogenating capacity of Rh favours the reduction of NO_3^-.

Regarding the behaviour of bimetallic catalysts, when the RhMo/G system (prepared by successive impregnations) was used, the activity for the elimination of NO_3^- was lower than that of the $RhMo_6$/G catalyst. The

Table 5 Concentration and selectivity to the products at the end of the reaction*

Catalyst	Final ppm NO_3^-	Final ppm NO_2^-	Final ppm NH_4^+	$S_{NO_2^-}$ %	$S_{NH_4^+}$ %	S_{N_2} %
Rh/G	50	1.7	0.15	3.5	0.3	96.2
Mo/G	100	–	–	–	–	–
RhMo/G	35	1.2	0.78	1.9	1.2	96.9
RhMo6/G	6	1.2	0.09	1.3	0.1	98.6

*The determinations were made at 300 min

selectivity to N_2 after 300 min of reaction for both bimetallic catalysts is listed in Table 5. Besides being more active, the $RhMo_6$/G catalyst gave a selectivity to N_2 higher than 98%, with a very low selectivity to NO_2^- and NH_4^+, showing that the Anderson phase is a more effective precursor for bimetallic catalysts.

4 Conclusions

Bimetallic $RhMo_6$ catalysts based on the adsorption of the Anderson-type planar heteropolymolybdate $[RhMo_6O_{24}H_6]^{3-}$ on alumina and silica-based supports were prepared, characterised and evaluated in the reaction leading to NO_3^- removal.

All the catalysts containing the $RhMo_6$ Anderson phase were active in the NO_3^- elimination in water. The $RhMo_6$/G catalyst (supported on γ-alumina) showed the best NO_3^- activity (94%) and selectivity to N_2, while for the $RhMo_6$/B catalyst (supported on boehmite-type alumina), the conversion was low (25%) with a behaviour similar to that of the monometallic Rh/G catalyst.

The catalytic performance (activity and selectivity to N_2) of all the systems studied depends on the concentration of adsorbed Rh and on the Rh/Mo surface ratio, which do not depend on the initial concentration of the starting solution but on the type of Anderson phase-support interaction.

The XPS and TPR analyses showed that the $RhMo_6$/G catalyst had a Rh/Mo surface ratio similar to that of the Anderson phase, indicating that this phase retained its structure up to the final stage of the preparation. $RhMo_6$/B showed a surface enrichment in Rh, indicating that in this case the structure of the Anderson phase was at least partially destroyed during the preparation.

The lower activity and selectivity to N_2 of a conventional RhMo/G catalyst prepared by the successive impregnation of Rh and Mo salts confirms that the heteropolyanion-support interaction generates an active surface with an ordered and uniform distribution of Rh and Mo on the support, causing a synergistic effect that favours the catalytic activity.

The results obtained indicate that Anderson-type heteropolyanion-based systems can be applied to aqueous phase hydrogenation reactions, particularly in the elimination of NO_3^- in water for human consumption. In addition, the use of these systems allow to obtain catalysts with a reproducible Rh/Mo ratio and a uniform active sites distribution.

Acknowledgements We are grateful to Mrs. Graciela Valle, Eng. Edgardo Soto, Lic. Mariela Theiller, Dra. Laura Barbelli and Eng. Hernán Bideberripe for their contribution and technical support.

Funding Information This study received financial support from the following institutions: CONICET (PIP 0276 and 0003), ANPCyT (PICT 0409) and UNLP (Subsidio Jóvenes Investigadores, Subsidio de Viajes) and Projects I172, X633 y X700; and CICPBA (Project 832/14).

References

Bae, S., Jung, J., & Lee, W. (2013). The effect of pH and zwitterionic buffers on catalytic nitrate reduction by TiO_2-supported bimetallic catalyst. *Chemical Engineering Journal, 232*, 327–337. https://doi.org/10.1016/j.cej.2013.07.099.

Barrabés, N., & Sá, J. (2011). Catalytic nitrate removal from water, past, present and future perspectives. *Applied Catalysis B: Environmental, 104*, 1–5. https://doi.org/10.1016/j.apcatb.2011.03.011.

Barrett, E. P., Joyner, L. G., & Halenda, P. P. (1951). The determination of pore volume and area distributions in porous substances. I. Computations from nitrogen isotherms. *Journal of the American Ceramic Society, 73*, 373–380.

Bertolini, G. R., Cabello, C. I., Muñoz, M., Casella, M., Gazzoli, D., Pettiti, I., & Ferraris, G. (2013). Catalysts based on Rh (III)-hexamolybdate/γ-Al_2O_3 and their application in the selective hydrogenation of cinnamaldehyde to hydrocinnamaldehyde. *Journal of Molecular Catalysis A: Chemical, 366*, 109–115. https://doi.org/10.1016/j.molcata.2012.09.013.

Bertolini, G. R., Vetere, V., Gallo, M. A., Muñoz, M., Casella, M. L., Gambaro, L., & Cabello, C. I. (2016). Composites based on modified clay assembled Rh (III)–heteropolymolybdates as catalysts in the liquid-phase hydrogenation of cinnamaldehyde. *Comptes Rendus Chimie, 19*(10), 1174–1183. https://doi.org/10.1016/j.crci.2015.09.015.

Bouras, O. (2003). Doctoral thesis, Université de Limoges, Faculté de Sciences et Techniques, Francia cap. 2.

Brunauer S, Emmett PH, Teller E (BET) method. (1985). In J. R. Anderson & K. C. Pratt (Eds.), *Introduction to characterization and testing of catalysts*. Australia: Academic Press.

Cabello, C. I., Botto, I. L., & Thomas, H. J. (1994). Reducibility and thermal behaviour of some Anderson phases. *Thermochimica Acta, 232*, 183–193. https://doi.org/10.1016/0040-6031(94)80058-8.

Cabello, C. I., Botto, I. L., & Thomas, H. J. (2000). Anderson type heteropolyoxomolybdates in catalysis: 1. $(NH_4)_3[CoMo_6O_{24}H_6]\cdot 7H_2O$/γ-$Al_2O_3$ as alternative of Co-Mo/γ-Al_2O_3 hydrotreating catalysts. *Applied Catalysis A: General, 197*, 79–86. https://doi.org/10.1016/S0926-860X(99)00535-9.

Cabello, C. I., Botto, I. L., Muñoz, M., & Thomas, H. (2002). Catalysts based on $RhMo_6$ heteropolymetallates. Bulk and supported preparation and characterization. *Studies in Surface Science and Catalysis, 143*, 565–573.

Cabello, C. I., Muñoz, M., Botto, I. L., & Payen, E. (2006). The role of Rh on a substituted Al Anderson heteropolymolybdate: thermal

and hydrotreating catalytic behaviour. *Thermochimia Acta., 447*, 22–29.

Choi, E., Park, K., Lee, H., Cho, M., & Ahn, S. (2013). Formic acid as an alternative reducing agent for the catalytic nitrate reduction in aqueous media. *Journal of Environmental Sciences, 25*, 1696–1702. https://doi.org/10.1016/S1001-0742(12)60226-5.

Citak, S., & Sonmez, S. (2010). Effects of conventional and organic fertilization on spinach (Spinacea oleracea L.) growth, yield, vitamin C and nitrate concentration during two successive seasons. *Scientia Horticulturae, 126*, 415–420. https://doi.org/10.1016/j.scienta.2010.08.010.

Costa, A. O., Ferreira, L. S., Passos, F. B., Maia, M. P., & Peixoto, F. C. (2012). Microkinetic modeling of the hydrogenation of nitrate in water on Pd–Sn/Al_2O_3 catalyst. *Applied Catalysis A: General, 445– 446*, 26–34.

Dalmon, J. A., & Martin, G. A. (1980). Hydrogenolysis of C_2H_6, C_3H_8 and n-C_4H_{10} over silica-supported nickel-copper catalysts. *Journal of Catalysis, 66*, 214–221. https://doi.org/10.1016/0021-9517(80)90023-8.

Ding, Y., Sun, W., Yang, W., & Li, Q. (2017). Formic acid as the in-situ hydrogen source for catalytic reduction of nitrate in water by PdAg alloy nanoparticles supported on amine-functionalized SiO_2. *Applied Catalysis B: Environmental, 203*, 372–380. https://doi.org/10.1016/j.apcatb.2016.10.048.

Fierro, J. L. G., Palacios, J. M., & Tomas, F. (1988). An analytical SEM and XPS study of platinum–rhodium gauzes used in high pressure ammonia burners. *Surface and Interface Analysis, 13*, 25–32. https://doi.org/10.1002/sia.740130107.

Gitzen, W. H. (Ed.). (1970). *Alumina as a ceramic material* (1st. ed.). Wiley-American Ceramic Society. https://doi.org/10.17226/9575.

Gurvitsch, L. (1914). Physicochemical attractive force. *Russian Journal of Physical Chemistry, 47*, 805–812.

Haber, F., Le Rossignol R. (1910). Production of ammonium, US Patent 971501.

Harkins, W. D., & Jura, G. (1994). Surfaces of solids. XIII. A vapor adsorption method for the determination of the area of a solid without the assumption of a molecular area, and the areas occupied by nitrogen and other molecules on the surface of a solid. *Journal of the American Ceramic Society, 66*, 1366–1376.

Jaworski, M. A., Vetere, V., Bideberripe, H. P., Siri, G., & Casella, M. L. (2013). Structural aspects of PtSn/γ-Al_2O_3 catalysts prepared through surface-controlled reactions: behavior in the water denitrification reaction. *Applied Catalysis A: General, 453*, 227–234. https://doi.org/10.1016/j.apcata.2012.12.034.

Kim, K. S., Baitinger, W. E., Amy, J. W., & Winograd, N. (1974). ESCA studies of metal-oxygen surfaces using argon and oxygen ion-bombardment. *Journal of Electron Spectroscopy and Related Phenomena, 5*, 351–367. https://doi.org/10.1016/0368-2048(74)85023-1.

Kim, Y.-N., Yeob Kim, M., & Choi, M. (2016). Synergistic integration of catalysis and ion-exchange for highly selective reduction of nitrate into N_2. *Chemical Engineering Journal, 289*, 423–432. https://doi.org/10.1016/j.cej.2016.01.002.

Lippens, B. J., & de Boer, J. H. (1965). Studies on pore systems in catalysts: V. The t method. *Journal of Catalysis, 4*, 319–323. https://doi.org/10.1016/0021-9517(65)90307-6.

Marchesini, F. A., Irusta, S., Querini, C., & Miró, E. (2008). Nitrate hydrogenation over Pt, In/Al_2O_3 and Pt, In/SiO_2. Effect of aqueous media and catalyst surface properties upon the catalytic activity. *Catalysis Communications, 9*, 1021–1026. https://doi.org/10.1016/j.catcom.2007.09.037.

Marchesini, F. A., Gutierrez, L. B., Querini, C. A., & Miró, E. E. (2010). Pt,In and Pd, In catalysts for the hydrogenation of nitrates and nitrites in water. FTIR characterization and reaction studies. *Chemical Engineering Journal, 159*, 203–211. https://doi.org/10.1016/j.cej.2010.02.056.

Mizuno, N., & Misono, M. (1998). Heterogeneous catalysis. *Chemical Reviews, 98*, 199–218. https://doi.org/10.1021/cr960401q.

Pettiti, I., Botto, I. L., Cabello, C. I., Colonna, S., Faticanti, M., Minelli, G., Porta, P., & Thomas, H. J. (2001). Anderson-type heteropolyoxomolybdates in catalysis: 2. EXAFS study on γ-Al_2O_3-supported Mo, Co and Ni sulfided phases as HDS catalysts. *Applied Catalysis A: General, 220*, 113–121. https://doi.org/10.1016/S0926-860X(01)00707-4.

Rinaldi, R., Fred, F. Y., & Schuchardt, U. (2006). Structural, morphological and acidic changes of nanocrystalline aluminas caused by a controlled humidity atmosphere. *Applied Catalysis A: General, 315*, 44–51. https://doi.org/10.1016/j.apcata.2006.08.032.

Soares, O., Órfão, J., Ruiz-Martínez, J., Silvestre-Albero, J., Sepúlveda-Escribano, A., & Pereira, M. F. R. (2010). Pd–Cu/AC and Pt–Cu/AC catalysts for nitrate reduction with hydrogen: Influence of calcination and reduction temperatures. *Chemical Engineering Journal, 165*, 78–88.

Thommes, M., & Cychosz, K. A. (2014). Physical adsorption characterization of nanoporous materials: progress and challenges. *Adsorption, 20*, 233–250. https://doi.org/10.1007/s10450-014-9606-z.

Thommes, M., Kaneko, K., Neimark, A. V., Olivier, J. P., Rodríguez-Reinoso, F., Rouquerol, J., & Sing, K. S. W. (2015). Physisorption of gases, with special reference to the evaluation of surface area and pore size distribution (IUPAC Technical Report). *Pure and Applied Chemistry, 87*(9–10), 1051.

Vieira Coelho, A. C., Rocha, G. A., Souza Santos, P., Souza Santos, H., & Kiyohara, P. K. (2008). Specific surface area and structures of aluminas from fibrillar pseudoboehmite. *Revista Matéria, 13*(2), 329.

Vorlop, K.-D., & Tacke, T. (1989). Kinetic investigation of the catalytic nitrate reduction: construction of the test reactor system. *Chemie Ingenieur Technik, 61*, 836–837. https://doi.org/10.1002/cite.330611023.

Wagner, C. D., Davis, L. E., Zeller, M. V., Taylor, J. A., Raymond, R. H., & Gale, L. H. (1981). Empirical atomic sensitivity factors for quantitative analysis by electron spectroscopy for chemical analysis. *Surface and Interface Analysis, 3*, 211–225. https://doi.org/10.1002/sia.740030506.

Zhao, J., & Chen, Q. (2003). Study on enhancement in gibbsite precipitation of Bayer process under 33 kHz ultrasound. *Journal of Materials Science and Technology, 19*, 607–610.

Zoppas, F. M., Marchesini, F. A., Devard, A., Bernardes, A. M., & Miró, E. E. (2016). Controlled deposition of Pd and In on carbon fibers by sequential electroless plating for the catalytic reduction of nitrate in water. *Catalysis Communications, 78*, 59–63. https://doi.org/10.1016/j.catcom.2016.02.012.